

$\Delta S^z=2$ quantum magnetization discontinuities proportional in number to the spin s in C_{60} : Origin and the role of symmetry

N. P. Konstantinidis

Department of Mathematics and Natural Sciences,

The American University of Iraq, Sulaimani,

Kirkuk Main Road, Sulaymaniyah, Kurdistan Region, Iraq

(Dated: today)

Abstract

The quantum antiferromagnetic Heisenberg model on the fullerene C_{60} in a magnetic field has $4s$ ground-state magnetization discontinuities with $\Delta S^z = 2$ as a function of the spin quantum number s that disappear at the classical limit. The molecule can be seen as the fullerene C_{20} with interpentagon interactions that generate the discontinuities when sufficiently strong. The discontinuities originate from the antiferromagnetic Ising limit for both molecules. The results show how spatial symmetry dictates the magnetic response of the I_h fullerene molecules.

PACS numbers: 75.10.Jm Quantized Spin Models, 75.50.Ee Antiferromagnetics, 75.50.Xx Molecular Magnets

I. INTRODUCTION

Fullerenes are allotropes of carbon whose most representative member is C_{60} [1–9]. C_{60} superconducts when doped with alkali metals [10]. Electron correlations are important for doped C_{60} , and they are accurately described within the framework of the Hubbard model (see [11] and references therein). According to estimates for the on-site repulsion U , C_{60} belongs to the intermediate- U regime of the Hubbard model [12–15], but its large U -limit, the Heisenberg model, is expected to qualitatively capture the spin correlations [16].

In the quantum antiferromagnetic Heisenberg model the total ground-state magnetization along an external field axis S^z changes discontinuously at specific field values typically by $\Delta S^z = 1$. In cases of spin-space anisotropy the energy is more efficiently minimized along certain directions, and this can lead to discontinuities with $\Delta S^z > 1$. It is of particular interest when such magnetization discontinuities occur in the absence of magnetic anisotropy. These are solely due to the frustrated connectivity of the magnetic interactions, directly reflecting the topology of the structure hosting the magnetic units.

The antiferromagnetic Heisenberg model has been extensively used to model the magnetic properties of low-dimensional frustrated topologies [17–22]. In fullerene molecules frustration is introduced by the twelve pentagons that each molecule has, with the number of hexagons increasing linearly with size [1]. The most symmetric fullerene molecules have icosahedral I_h symmetry like C_{60} . These are minimally frustrated among the fullerenes if one excludes the Platonic solid dodecahedron [23–26] that only has pentagons [27, 28], and have also been found to share the ground-state magnetic response. At the classical level there are two magnetization discontinuities in an external field when all exchange interactions are equal, with the exception of the dodecahedron that has three [16, 29, 30]. In the extreme quantum limit where the individual spin magnitude $s = \frac{1}{2}$ and 1, the dodecahedron has respectively one and two discontinuities with $\Delta S^z = 2$ [29]. A high-field ground-state magnetization jump with $\Delta S^z = 2$ was established to be a common feature of the I_h fullerenes for $s = \frac{1}{2}$ when all exchange interactions are equal [30]. For I_h -fullerenes bigger than the dodecahedron it is not possible to calculate the magnetic response for not-so-high S^z due to computational limitations imposed by the size of the Hilbert space. Relatively small fullerene molecules with different symmetry have only pronounced magnetization plateaus when $s = \frac{1}{2}$ [31, 32]. Magnetization discontinuities with $\Delta S^z > 1$ have also been observed in the case of extended systems [33–40].

The dual of the dodecahedron, the icosahedron, has also been shown to possess a magnetization

discontinuity at the classical lowest-energy configuration in an external field, which disappears at the extreme quantum limit [41]. This discontinuity can be understood from a structural point of view, as the icosahedron can be viewed as a closed strip of a triangular lattice with two additional spins attached [42]. Such a structural explanation of the magnetization discontinuities is not obvious for the dodecahedron. It can neither apply to the discontinuities of fullerene molecules where all pentagons are located at their ends and their body has the form of a nanotube, comprising only of hexagons [11].

To investigate the origin of the $\Delta S^z = 2$ magnetization discontinuities of the dodecahedron for $s = \frac{1}{2}$ and 1 the quantum anisotropic Heisenberg model (AHM) is considered. Its antiferromagnetic isotropic limit is approached from the corresponding Ising limit by gradually increasing the strength of the interactions in the xy plane. Karřová *et al.* calculated the ground-state magnetization response of the $s = \frac{1}{2}$ AHM on the dodecahedron for different values of the anisotropy [43], extending the calculation done at the isotropic limit [29]. In the present paper it is shown that there is a strong ground-state magnetization discontinuity at the antiferromagnetic Ising limit at the saturation field. This discontinuity is very closely monitored as the fluctuations in the xy plane are switched on. Degenerate perturbation theory on the xy -plane interactions shows that the saturation-field jump develops into the $\Delta S^z = 2$ high-field magnetization discontinuity five spin-flips away from saturation for any finite s , with the discontinuity disappearing at the classical limit $s \rightarrow \infty$, demonstrating its pure quantum nature. Then evolving continuously away from the antiferromagnetic Ising limit by increasing the strength of the xy coupling shows that the jump survives beyond the isotropic Heisenberg limit for $s = \frac{1}{2}$ and 1. For increasingly higher s the xy -plane fluctuations are strong enough to confine the discontinuity closer and closer to the Ising limit.

The calculation is then extended to the next-bigger I_h fullerene, the truncated icosahedron C_{60} , which has also been found to support the $\Delta S^z = 2$ ground-state magnetization discontinuity five spin flips away from saturation for $s = \frac{1}{2}$ and uniform interactions [30]. Here the relative strength of the two symmetrically independent interactions is allowed to vary and relates to how strongly neighboring pentagons are coupled, since they are isolated from one another and do not share any vertices or edges, as in the dodecahedron. Degenerate perturbation theory shows that the $\Delta S^z = 2$ discontinuity is again generated infinitesimally away from the antiferromagnetic Ising limit for arbitrary s if the interpentagon coupling is at least equal to $\tan^{-1}(0.01143\pi)$ times the intrapentagon one. However, its existence at the antiferromagnetic isotropic limit requires the two couplings to be roughly equal in order for the $\Delta S^z = 2$ discontinuity to survive for $s = \frac{1}{2}$.

Increasing s again works against the discontinuity, but making the interpentagon coupling strong enough allows the jump to appear for arbitrary s , with the required minimum interpentagon coupling increasing with s and the AHM approaching closer and closer its strong interpentagon-coupling or dimer limit. This demonstrates that C_{60} can behave like its smaller symmetric relative, C_{20} , if the interpentagon interactions are strong enough, and shows the close connection between symmetry and magnetic properties. Furthermore since the next-bigger I_h fullerene, the chamfered dodecahedron [1], also has a $\Delta S^z = 2$ five-spin-flips away from saturation ground-state jump in a magnetic field for $s = \frac{1}{2}$ when its two symmetrically unique interactions are equal [30], it is expected that bigger molecules with I_h symmetry will follow the discontinuity pattern of C_{60} . In their case the interpentagon coupling is mediated by exchange interactions of one or more kinds. The similarities in the ground-state magnetic response of the I_h fullerene molecules demonstrate a strong correlation between symmetry and magnetic behavior for this family, which can allow the prediction of the properties of larger molecules, which are impossible to treat numerically, from the ones of their smaller relatives.

In order to investigate in more detail the behavior close to the dimer limit where the $\Delta S^z = 2$ ground-state discontinuity is favored and the interpentagon is much stronger than the intrapentagon interaction, degenerate perturbation theory on the latter is considered for arbitrary s . The Hilbert space of the AHM on C_{60} is enormous, however degenerate perturbation theory allows the calculation of the lowest energies for the whole range of S^z in this limit, as long as s is not too big. C_{60} then reduces to an icosidodecahedron of dimers interacting weakly with one another. For $s = \frac{1}{2}$ it is found that apart from the five-spin-flips away from saturation $\Delta S^z = 2$ discontinuity at the isotropic AHM limit, another one exists at low fields with the $S^z = 5$ sector never including the ground state in a field. This is a manifestation of the singlet-triplet or hole-particle symmetry between low and high magnetic fields after the projection to the lowest-energy singlet and triplet states of the dimers has been made [44–46]. Degenerate perturbation theory for arbitrary s shows that the number of $\Delta S^z = 2$ ground-state discontinuities grows as $4s$, with the pattern of lower and higher-field jumps repeating in the magnetization curve $2s$ times and disappearing at the classical limit. These discontinuities are expected to survive away from the dimer limit, as has been shown for the one close to saturation, and show how insight on the magnetic response for lower- S^z sectors not directly accessible with diagonalization can be deduced by degenerate perturbation theory on the dimer limit. Again, since symmetry and strong interpentagon coupling are important for the appearance of the jumps, it is expected that the latter will be general features of the I_h -fullerene molecules.

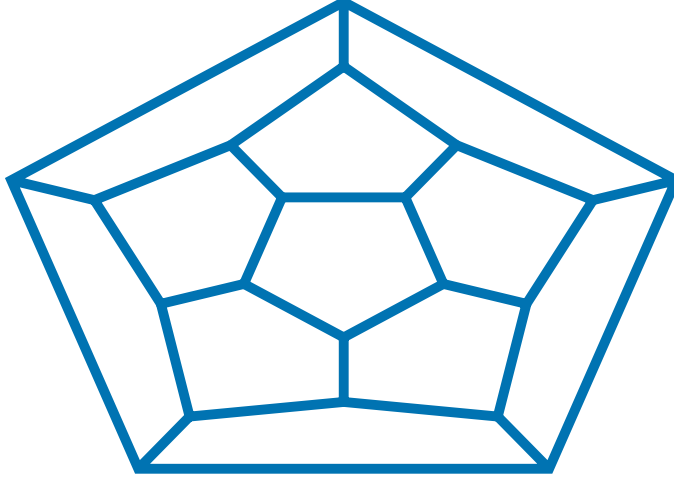


FIG. 1: Planar projection of the dodecahedron C_{20} .

II. MODEL

The Hamiltonian of the quantum AHM in a magnetic field \vec{h} with a single spin \vec{s}_i , $i = 1, \dots, N$ located on each of the N vertices of a molecule is

$$H = \sum_{\langle ij \rangle} J_{ij} \left[\sin \omega \left(s_i^x s_j^x + s_i^y s_j^y \right) + \cos \omega s_i^z s_j^z \right] - h \sum_{i=1}^N s_i^z. \quad (1)$$

The symbol $\langle \rangle$ indicates that interactions are limited to nearest-neighbors and have strength equal to J_{ij} for spins i and j connected by an edge of the molecule. The Ising coupling along the z axis is scaled with $\cos \omega$ and the coupling in the xy plane with $\sin \omega$, and $0 \leq \omega < \frac{3}{4}\pi$ is taken. The antiferromagnetic limits are the Ising for $\omega = 0$, the isotropic Heisenberg for $\omega = \frac{\pi}{4}$, and the XX for $\omega = \frac{\pi}{2}$. The interactions are taken to obey the molecular symmetry, with two edges connected by a symmetry operation of the I_h point group corresponding to the same interaction strength. The magnetic field is directed along the z axis. Hamiltonian (1) is block-diagonalized by taking into account S^z and its spatial and spin symmetries, and the lowest-lying level in each sector is then found with Lanczos diagonalization [29]. At the Ising limit the lowest-energy states of Hamiltonian (1) in the different S^z sectors are degenerate. It is also possible to perturb away from this limit with the interactions in the xy plane by simultaneously taking the Hamiltonian symmetries into account, and calculate the first-order energy correction with degenerate perturbation theory [47, 48].

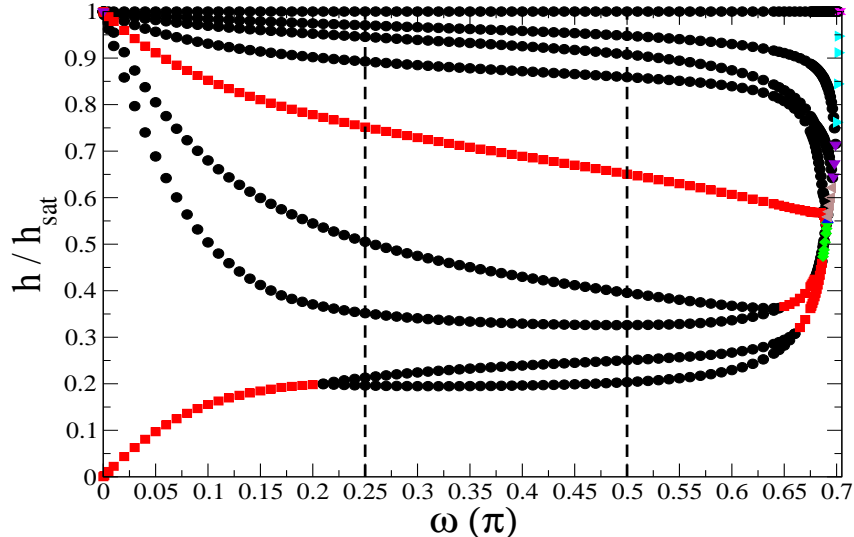


FIG. 2: Magnetic fields h over the saturation field h_{sat} for which ground-state magnetization discontinuities occur as a function of ω in the ground state of Hamiltonian (1) for C_{20} for $s = \frac{1}{2}$. The (black) circles correspond to discontinuities with $\Delta S^z = 1$, the (red) squares with $\Delta S^z = 2$, the (green) diamonds with $\Delta S^z = 3$, the (blue) triangles up with $\Delta S^z = 6$, the (brown) triangles left with $\Delta S^z = 7$, the (violet) triangles down with $\Delta S^z = 8$, the (cyan) triangles right with $\Delta S^z = 9$, and the (magenta) \times 's with $\Delta S^z = 10$. The (black) dashed lines show the isotropic Heisenberg ($\omega = \frac{\pi}{4}$) and the XX ($\omega = \frac{\pi}{2}$) limit.

III. DODECAHEDRON C_{20}

The dodecahedron, whose planar projection is shown in Fig. 1, is a Platonic solid [23], and all its $N = 20$ vertices are geometrically equivalent. It consists of twelve pentagons, and is the smallest fullerene in the form of C_{20} [1, 24–26]. All of its edges are symmetrically equivalent, making all bonds J_{ij} in Hamiltonian (1) equal, and it is taken $J_{ij} \equiv 1$ from now on. At the antiferromagnetic Ising limit $\omega = 0$ the lowest energy of Hamiltonian (1) belongs to both the $S^z = 0$ and $4s$ subsectors, making the lowest-lying levels from $S^z = 1$ to $4s - 1$ excited (Tables I, II, and III). The ground-state energy as a function of S^z is linear, resulting in a strong magnetization jump $\Delta S^z = 16s$ to saturation (Figs 2 and 3).

Perturbing away from the Ising limit with the interactions in the xy plane in first order ($\omega \rightarrow 0$) decreases the $S^z = 0$ -energy but not the $S^z = 4s$ for $s = \frac{1}{2}$ (Table I), resulting in a low-field $\Delta S^z = 4s$ magnetization jump (Fig. 2). For $s = 1$ and $\frac{3}{2}$ first-order perturbation theory does not resolve this degeneracy (Tables II and III), but Lanczos diagonalization shows that the low-field $\Delta S^z = 4s$ discontinuity also occurs when $s = 1$ (Fig. 3). Magnetization jumps occur when the

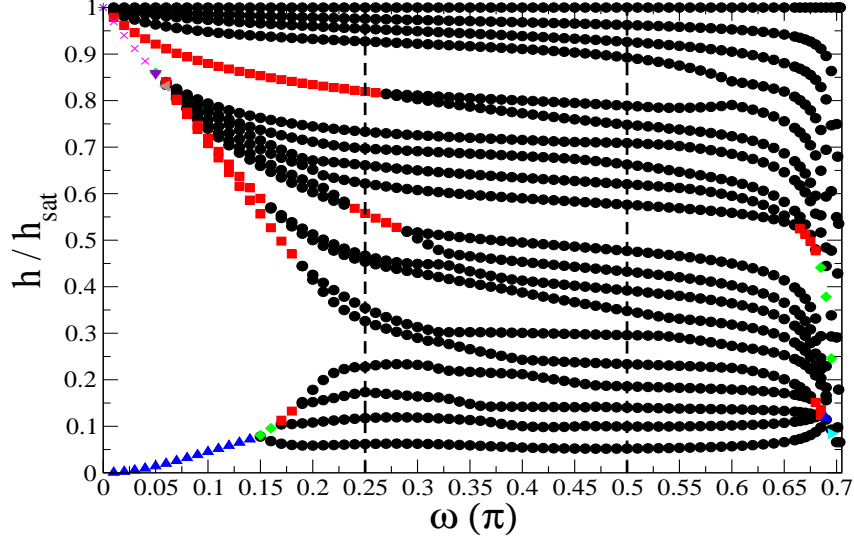


FIG. 3: Magnetic fields h over the saturation field h_{sat} for which ground-state magnetization discontinuities occur as a function of ω in the ground state of Hamiltonian (1) for C_{20} for $s = 1$. The (black) circles correspond to discontinuities with $\Delta S^z = 1$, the (red) squares with $\Delta S^z = 2$, the (green) diamonds with $\Delta S^z = 3$, the (blue) triangles up with $\Delta S^z = 4$, the (brown) triangles left with $\Delta S^z = 6$, the (violet) triangles down with $\Delta S^z = 7$, the (cyan) triangles right with $\Delta S^z = 9$, the (magenta) \times 's with $\Delta S^z = 10$, and the (indigo) stars with $\Delta S^z = 16$. The (black) dashed lines show the isotropic Heisenberg ($\omega = \frac{\pi}{4}$) and the XX ($\omega = \frac{\pi}{2}$) limit.

energy differences between the lowest-energy states of successive S^z sectors do not increase with increasing S^z . Since the ground-state energy varies linearly with S^z at the unperturbed limit, the energy differences between the lowest-energy levels in successive S^z sectors are determined by the perturbative corrections. That first-order perturbation theory can not resolve the degeneracies away from the high- S^z region is also demonstrated by the high degeneracy of the energy corrections in Tables II and III, which belong to multiple irreducible representations [49]. First-order perturbation theory shows the existence of a magnetization jump between $4s$ and $Ns - 6$ for $s = 1$ and $\frac{3}{2}$. Fig. 3 shows that the jump survives for higher values of ω for $s = 1$.

In contrast to the perturbative results for lower S^z , from $S^z = Ns - 6$ to saturation the lowest-energy states belong to a single irreducible representation, which does not change with increasing s . The first-order perturbative corrections in these S^z sectors are multiples of s (Table IV), making the magnetization response close to saturation the same for any s . Calculating the energy differences between the high-field successive sectors shows that the $S^z = Ns - 5$ sector, the one with five spin-flips away from saturation, never becomes the ground state in the field, irrespective of s ,

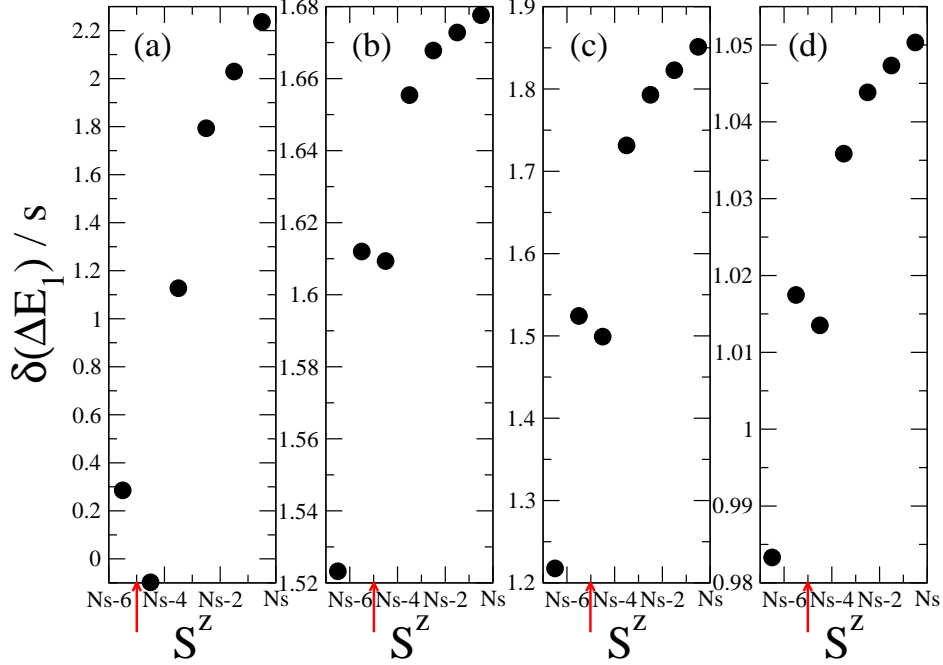


FIG. 4: Differences of the first-order degenerate perturbation theory corrections of the energy over the spin magnitude $\frac{\delta(\Delta E_1)}{s} = \frac{\Delta E_1(S^z+1)}{s} - \frac{\Delta E_1(S^z)}{s}$ between successive S^z sectors close to saturation for arbitrary s for (a) C_{20} (Table IV) and (b), (c), and (d) for C_{60} for $\phi = \frac{\pi}{50}, \frac{\pi}{4},$ and $\frac{49}{100}\pi$ respectively (Table VI) away from the Ising limit $\omega = 0$ of Hamiltonian (1) for $h = 0$. The (red) solid arrows show the locations of the $\Delta S^z = 2$ magnetization discontinuities.

resulting in a $\Delta S^z = 2$ discontinuity (Fig. 4(a)). The energy differences between the sectors scale with s , while the energies at the classical limit scale as s^2 , showing that the discontinuity is a pure quantum effect which occurs for arbitrary finite s , but disappears at the classical limit $s \rightarrow \infty$. It is noted that for every $s = 1$ -level with $4s < S^z < Ns - 6$ there is a corresponding $s = \frac{3}{2}$ -level in the analogous S^z range so that the ratio of their first-order perturbative energy corrections equals the ratio of their s values.

The dodecahedron is small enough to calculate the lowest-energy state in each S^z -sector with Lanczos diagonalization for $s = \frac{1}{2}$ and 1, allowing to monitor the evolution of all magnetization discontinuities away from first-order perturbation theory on the antiferromagnetic Ising limit. The magnetization response for $s = \frac{1}{2}$ and 1 is shown in Figs 2 and 3, with the magnetization curves for $\omega = \frac{\pi}{20}, \frac{\pi}{4},$ and $\frac{\pi}{2}$ plotted in Figs 5 and 6. Karřlová *et al.* have provided the plot for $s = \frac{1}{2}$ up to $\omega = \frac{\pi}{4}$ [43]. As the coupling in the xy plane gets stronger the high-field discontinuity survives at the isotropic Heisenberg limit $\omega = \frac{\pi}{4}$ for both values of s . The other discontinuities disappear, with the exception of a $\Delta S^z = 2$ discontinuity around $S^z = 9$ for $s = 1$, that reenters a little before

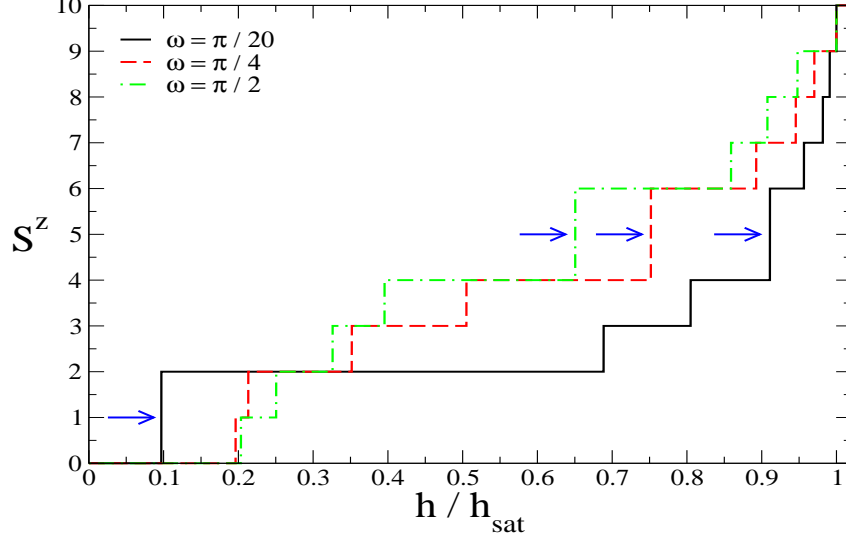


FIG. 5: S^z as a function of the magnetic field h over the saturation field h_{sat} in the ground state of Hamiltonian (1) for C_{20} for $s = \frac{1}{2}$. The (black) solid line corresponds to $\omega = \frac{\pi}{20}$, the (red) long-dashed line to $\omega = \frac{\pi}{4}$, and the (green) long-dashed-dotted line to $\omega = \frac{\pi}{2}$. The (blue) solid arrows point to the discontinuities with $\Delta S^z = 2$.

TABLE I: Hamiltonian (1) with $h = 0$ for C_{20} for $s = \frac{1}{2}$. The columns list the sector S^z , the lowest energy E_0 at the Ising limit $\omega = 0$, its degeneracy (deg.), the first-order degenerate perturbation theory energy correction ΔE_1 on ω , its degeneracy (deg.), and the irreducible representation (irrep.) of the I_h symmetry group it belongs. ΔE_1 has been calculated with double-precision accuracy but less digits are shown.

S^z	E_0	deg.	ΔE_1	deg.	irrep.
0	$-\frac{9}{2}$	240	$-(\sqrt{3} + \frac{1}{2})$	1	A_u
1	-4	900	-2.64146	3	T_{2u}
2	$-\frac{9}{2}$	5	0	5	A_g, F_g
3	-3	320	-2.56533	4	F_u
4	$-\frac{3}{2}$	1240	-3.68687	1	A_g
5	0	1912	-3.54419	4	F_g
6	$\frac{3}{2}$	1510	-3.59294	1	A_u
7	3	660	-3.02938	3	T_{1u}
8	$\frac{9}{2}$	160	-2.13276	5	H_g
9	6	20	$-\frac{\sqrt{5}}{2}$	3	T_{2u}
10	$\frac{15}{2}$	1	0	1	A_g

the isotropic limit and traces back to the $\Delta S^z = 10$ discontinuity of weak ω .

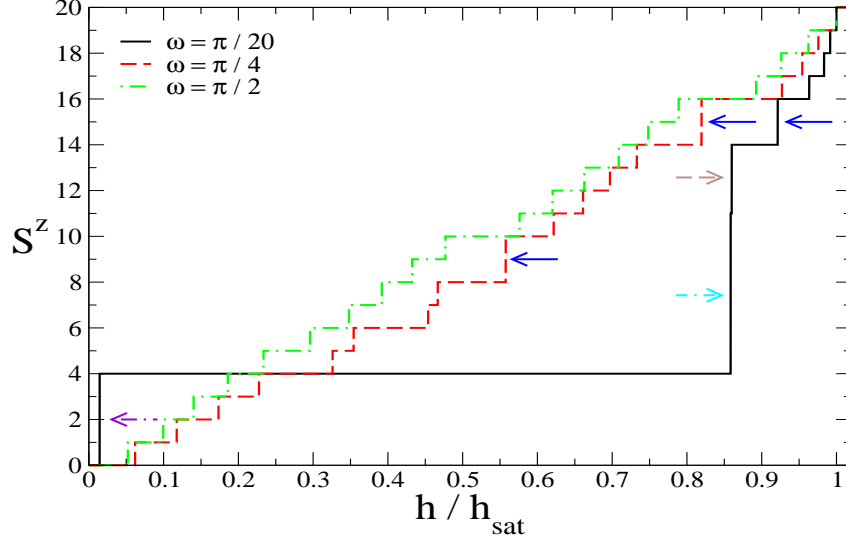


FIG. 6: S^z as a function of the magnetic field h over the saturation field h_{sat} in the ground state of Hamiltonian (1) for C_{20} for $s = 1$. The (black) solid line corresponds to $\omega = \frac{\pi}{20}$, the (red) long-dashed line to $\omega = \frac{\pi}{4}$, and the (green) long-dashed-dotted line to $\omega = \frac{\pi}{2}$. The (blue) solid arrows point to the discontinuities with $\Delta S^z = 2$, the (brown) long-dashed arrow to the discontinuity with $\Delta S^z = 3$, the (violet) long-dashed-dotted arrow to the discontinuity with $\Delta S^z = 4$, and the (cyan) double-dashed-dotted arrow to the discontinuity with $\Delta S^z = 7$.

Monitoring the $\Delta S^z = 2$ discontinuities away from the isotropic limit for higher ω shows that the two $s = 1$ jumps quickly disappear, while the $s = \frac{1}{2}$ discontinuity survives up to the XX limit where $\omega = \frac{\pi}{2}$ and the Ising interaction is zero. Further increasing ω makes the interaction along the z axis ferromagnetic, and eventually the discontinuity disappears at $\omega = 0.68562\pi$. The detrimental effect of the xy -plane fluctuations on the $\Delta S^z = 2$ discontinuity away from the Ising limit is getting stronger with s as shown in Fig. 7, which plots the highest ω value for which the jump survives as a function of s (Table V). The jump does not survive at the isotropic Heisenberg limit for $s > 1$.

IV. TRUNCATED ICOSAHEDRON C_{60}

The truncated icosahedron, whose planar projection is shown in Fig. 8, has $N = 60$ and is an Archimedean solid [50], having all vertices geometrically equivalent and two different types of polygons, pentagons and hexagons. It is the most representative fullerene in the form of C_{60} [1–8]. It has two symmetrically unique types of edges, which correspond to two independent

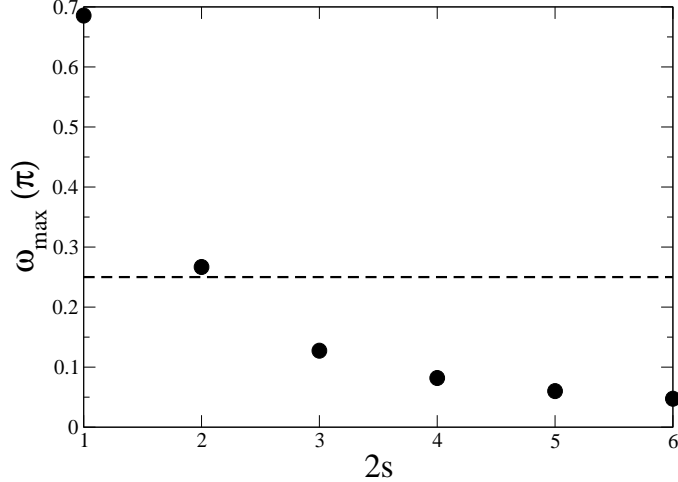


FIG. 7: Maximum value ω_{max} as a function of s for which the ground state of Hamiltonian (1) for C_{20} has a $\Delta S^z = 2$ magnetization discontinuity five spin flips away from saturation. The dashed line shows the isotropic Heisenberg limit $\omega = \frac{\pi}{4}$.

exchange interactions in Hamiltonian (1). The first type links vertices of the same pentagon and is taken to have strength $J_1 \equiv \cos\phi$ (blue thick lines in Fig. 8), while the second vertices that belong to different pentagons and has strength $J_2 \equiv \sin\phi$ (red thin lines in Fig. 8) with $0 \leq \phi \leq \frac{\pi}{2}$, interpolating between isolated pentagons and isolated dimers. Unlike the dodecahedron the pentagons do not share vertices but rather interact via the interpentagon bonds, which represent the interaction strength between neighboring pentagons.

Very close to the isolated pentagon limit ϕ is small and first-order degenerate perturbation theory away from the Ising limit shows that there is no $\Delta S^z = 2$ ground-state discontinuity five spin flips away from saturation. A minimum value of ϕ is required for the discontinuity to appear within first-order perturbation theory, and it exists for $\phi \geq 0.01143\pi$ for arbitrary s . Table VI lists the first-order perturbation theory corrections away from the antiferromagnetic Ising limit $\omega = 0$ for arbitrary s , higher S^z and three different values of ϕ : one close to the isolated pentagon limit $J_2 \ll J_1$ ($\phi = \frac{\pi}{50}$), one corresponding to uniform exchange interactions ($\phi = \frac{\pi}{4}$), and one close to the dimer limit $J_2 \gg J_1$ ($\phi = \frac{49}{100}\pi$). Like for the dodecahedron, the sector with five spin-flips from saturation is never the ground state in a magnetic field (Figs 4(b), (c), and (d)). The $\Delta S^z = 2$ discontinuity of the dodecahedron is inherited from the truncated icosahedron, which shares its spatial symmetry, within first-order degenerate perturbation theory away from the Ising limit, as long as the interpentagon coupling is not very small. Further evidence to that is provided by the irreducible representations that include the lowest-energy state in each S^z sector, which are very

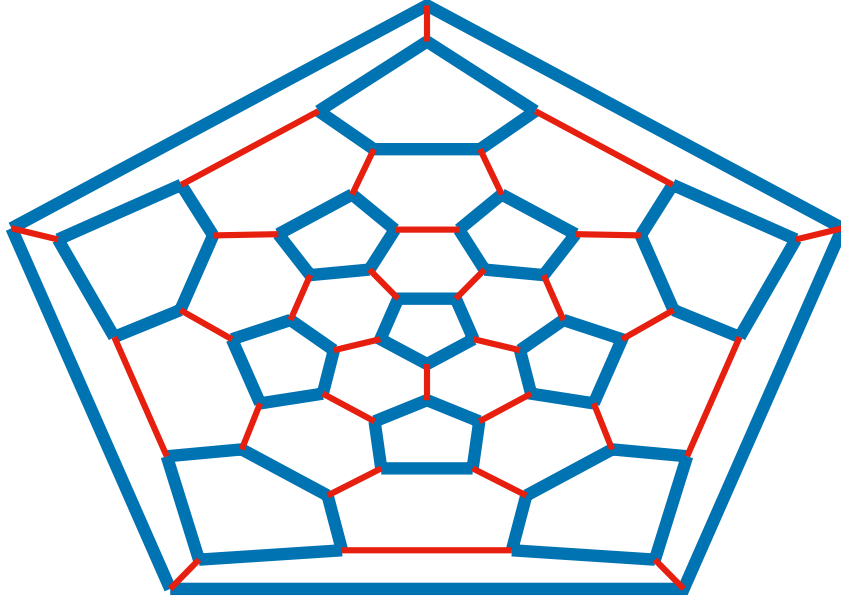


FIG. 8: Planar projection of the truncated icosahedron C_{60} . The (blue) thick lines correspond to the twelve pentagons and the intrapentagon bonds and their exchange interaction strength $J_1 \equiv \cos\phi$, while the (red) thin lines to the interpentagon (dimer) bonds and their exchange interaction strength $J_2 \equiv \sin\phi$.

similar for the two molecules.

For the dodecahedron it was found that the fluctuations around the Ising axis work against the $\Delta S^z = 2$ ground-state magnetization discontinuity, and eventually a sufficiently strong value of ω makes the discontinuity disappear. The same is true for the truncated icosahedron, and Fig. 9 plots the maximum value ω_{max} for which the $\Delta S^z = 2$ magnetization discontinuity exists as a function of ϕ for s up to $\frac{3}{2}$ (the corresponding data is listed in Table VII and have been calculated with Lanczos diagonalization). For $\phi < 0.01143\pi$ it takes a minimum value ω_{min} for the jump to appear, and ω_{max} is small and slightly decreases with ϕ . The ω_{min} values are listed in Table VIII for $s = \frac{1}{2}$, 1, and $\frac{3}{2}$. Within the accuracy of the calculation they are inversely proportional to $2s$. As ϕ increases the interpentagon bonds get stronger at the expense of the intrapentagon bonds, resulting in a discontinuity that survives up to higher values of ω , until a sufficiently strong ϕ supports the jump up to the isotropic limit $\omega = \frac{\pi}{4}$.

The ω_{max} value for which the discontinuity survives decreases with s for fixed ϕ according to Fig. 9, showing that the interactions in the xy plane are becoming more detrimental to the jump with increasing s , as has also been found for the dodecahedron. Simultaneously, the required minimum value ϕ_{min} for the jump to survive at the isotropic Heisenberg limit increases with s , and is already close to $\frac{\pi}{2}$ for $s = \frac{3}{2}$ (Fig. 10 and Table IX). These results demonstrate that the stronger

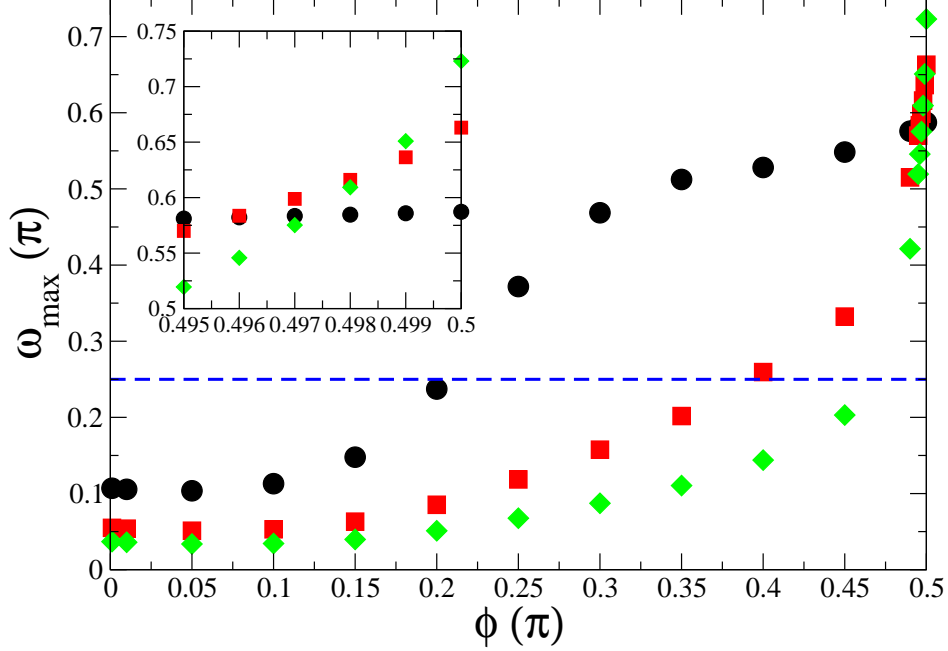


FIG. 9: Maximum value ω_{max} for which the $s = \frac{1}{2}$ (black circles), 1 (red squares), and $\frac{3}{2}$ (green diamonds) ground state of Hamiltonian (1) for C_{60} has a $\Delta S^z = 2$ magnetization discontinuity between $S^z = Ns - 6$ and $Ns - 4$ as a function of $\phi = \tan^{-1} \frac{J_2}{J_1}$, which determines the relative strength of the two symmetrically independent exchange interactions. The dashed line shows the isotropic Heisenberg limit $\omega = \frac{\pi}{4}$. The inset focuses on the high range of ϕ .

the interaction between the pentagons the more “dodecahedron-like” the truncated icosahedron becomes in terms of $\Delta S^z = 2$ discontinuous ground-state magnetic response. They also explain the common magnetic properties of the two molecules, and also point to a similar mechanism for bigger I_h fullerenes that also share these properties [30].

The inset of Fig. 9 focuses on values of ϕ close to $\frac{\pi}{2}$. Contrary to what happens for smaller ϕ , ω_{max} increases with s as ϕ approaches $\frac{\pi}{2}$. When $\phi \rightarrow \frac{\pi}{2}$ the truncated icosahedron reduces to 30 dimers perturbatively coupled via intrapentagon bonds, which form an icosidodecahedron. First-order degenerate perturbation theory gives the lowest-energy correction ΔE_1 at the isotropic Heisenberg limit $\omega = \frac{\pi}{4}$ for every S^z sector, and not only close to saturation as with Lanczos diagonalization, as long as s is not too big (Tables X, XI, and XII). Figure 11 plots the differences $\delta(\Delta E_1)$ between successive S^z sectors (App. A). These typically increase with S^z , resulting in magnetization jumps $\Delta S^z = 1$. For S^z sectors which are multiples of 5 the dependence of $\delta(\Delta E_1)$ on S^z is not as smooth, and in particular around the sectors $S^z = \frac{N}{2}i + 5$ and $S^z = \frac{N}{2}(i + 1) - 5$ with $i = 0, 1, \dots, 2s - 1$ $\delta(\Delta E_1)$ decreases with S^z . These sectors never include the ground state

in a magnetic field, resulting in a number of $4s$ discontinuities as a function of s with $\Delta S^z = 2$. These are sectors with an S^z value differing by 5 from sectors whose S^z is an integer multiple of $\frac{N}{2}$. The appearance of $\Delta S^z = 2$ ground-state discontinuities in pairs for regions of S^z where $\frac{N}{2}i \leq S^z \leq \frac{N}{2}(i+1)$ originates from the hole-particle symmetry with respect to the center of the region, after the projection to the lowest-energy dimer states has been made [44–46]. Since Lanczos diagonalization shows that the $\Delta S^z = 2$ discontinuity five spin flips away from saturation is present at the isotropic Heisenberg limit away from the perturbative dimer limit the further the smaller s is, it is expected that the other discontinuities can also survive relatively far from the strong dimer limit, allowing to infer the magnetic response for not-so-high S^z , where the Hilbert space is enormous, from the dimer limit where the size of the Hilbert space is tractable. Table XIII lists the ω_{max} values for the different discontinuities when $\phi \rightarrow \frac{\pi}{2}$, which increase with s as was also found in the inset of Fig. 9. Each value belongs to a pair of discontinuities.

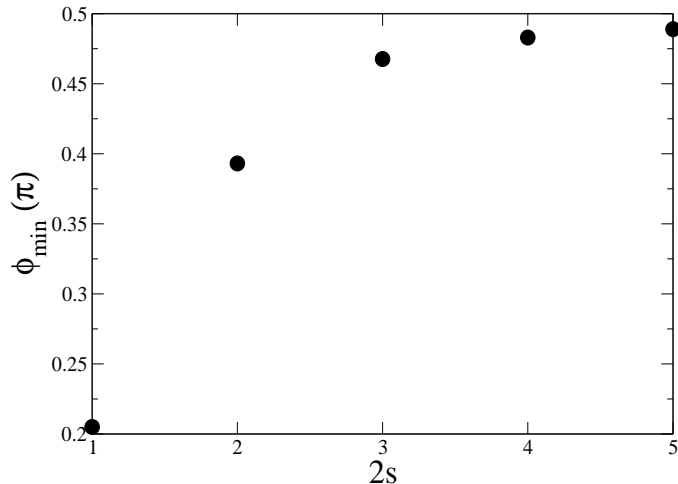


FIG. 10: Minimum value ϕ_{min} as a function of s for which the ground state of Hamiltonian (1) for C_{60} has a $\Delta S^z = 2$ magnetization discontinuity five spin flips away from saturation at the isotropic Heisenberg limit $\omega = \frac{\pi}{4}$.

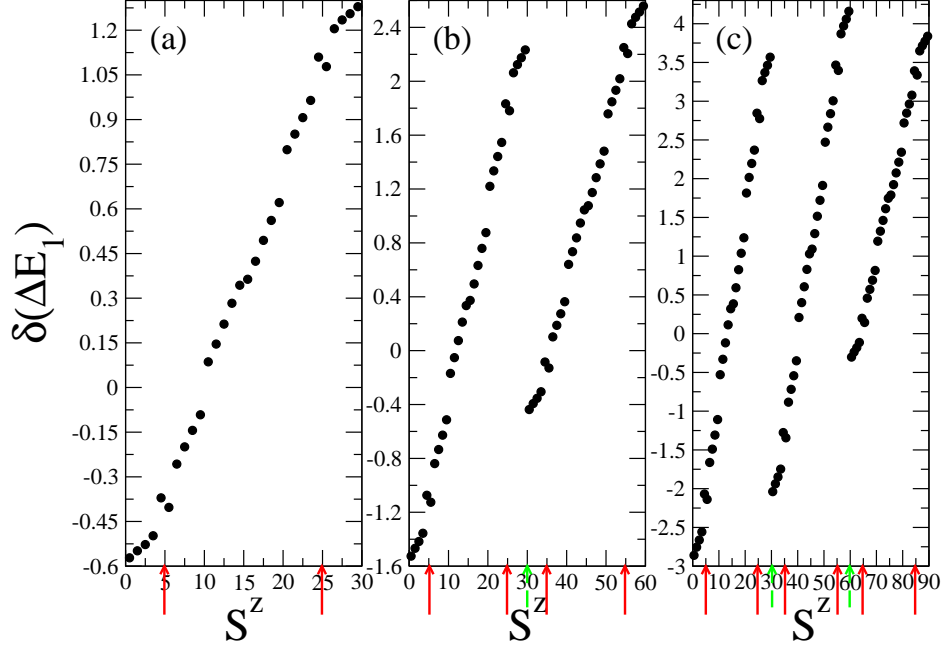


FIG. 11: Differences of the first-order degenerate perturbation theory corrections of the energy $\delta(\Delta E_1) = \Delta E_1(S^z + 1) - \Delta E_1(S^z)$ between successive S^z sectors of C_{60} away from the dimer limit $\phi = \frac{\pi}{2}$ at the antiferromagnetic isotropic Heisenberg limit $\omega = \frac{\pi}{4}$ of Hamiltonian (1) for $h = 0$ and (a) $s = \frac{1}{2}$ (ΔE_1 given in Table X), (b) $s = 1$ (ΔE_1 given in Table XI), and (c) $s = \frac{3}{2}$ (ΔE_1 given in Table XII). The (red) solid arrows show the locations of the $\Delta S^z = 2$ magnetization discontinuities, and the (green) long-dashed arrows the locations of standard $\Delta S^z = 1$ discontinuities which are due to the unperturbed energies (App. A).

TABLE II: Same as Tab. I for $s = 1$.

S^z	E_0	deg.	ΔE_1	deg.	irrep.	S^z	E_0	deg.	ΔE_1	deg.	irrep.
0	-18	240	0	240	all	11	3	41120	-4.20815	30	all but A_g, A_u
1	-17	1440	-2	60	all but A_g	12	6	41475	-5.22625	10	A_g, F_g, H_g
2	-16	4080	-3.81284	30	all but T_{1g}, T_{2g}, A_u	13	9	32920	-6.25465	20	$A_g, F_g, H_g,$ T_{1u}, T_{2u}, F_u
3	-17	60	-1	30	all but A_g, A_u	14	12	20520	-7.37374	1	A_g
4	-18	5	0	5	A_g, F_g	15	15	9932	-7.08838	4	F_g
5	-15	40	0	40	all	16	18	3650	-7.18588	1	A_u
6	-12	460	0	460	all	17	21	980	-6.05876	3	T_{1u}
7	-9	2520	$-\sqrt{2}$	60	all but A_u	18	24	180	-4.26553	5	H_g
8	-6	8310	$-\sqrt{5}$	120	all	19	27	20	$-\sqrt{5}$	3	T_{2u}
9	-3	18920	-3.12602	40	all	20	30	1	0	1	A_g
10	0	31852	-3.62611	120	all						

TABLE III: Same as Tab. I for $s = \frac{3}{2}$.

S^z	E_0	deg.	ΔE_1	deg.	irrep.	S^z	E_0	deg.	ΔE_1	deg.	irrep.
0	-40.5	240	0	240	all	16	4.5	250840	-4.78375	30	all but T_{1g}, T_{2g}, A_u
1	-39	1440	$-\frac{3}{2}$	720	all	17	9	301680	-5.43916	120	all
2	-37.5	4320	-3	720	all	18	13.5	320160	-6.24360	120	all
3	-36	9980	$-\frac{9}{2}$	340	all	19	18	300400	-6.31222	30	all but A_g, A_u
4	-37.5	360	-3	75	all	20	22.5	249032	-7.83938	10	A_g, F_g, H_g
5	-39	60	$-\frac{3}{2}$	30	all but A_g, A_u	21	27	181860	-7.83938	20	A_g, F_g, H_g T_{1u}, T_{2u}, F_u
6	-40.5	5	0	5	A_g, F_g	22	31.5	116315	-9.38197	20	A_g, F_g, H_g T_{1u}, T_{2u}, F_u
7	-36	40	0	40	all	23	36	64560	-9.38197	20	A_g, F_g, H_g T_{1u}, T_{2u}, F_u
8	-31.5	180	0	180	all	24	40.5	30680	-11.06061	1	A_g
9	-27	880	0	880	all	25	45	12232	-10.63257	4	F_g
10	-22.5	3570	0	3570	all	26	49.5	3970	-10.77881	1	A_u
11	-18	11480	$-\frac{3}{2}\sqrt{2}$	60	all but A_u	27	54	1000	-9.08814	3	T_{1u}
12	-13.5	29800	$-\frac{3}{2}\sqrt{2}$	360	all	28	58.5	180	-6.39829	5	H_g
13	-9	64040	$-\frac{3}{2}\sqrt{5}$	120	all	29	63	20	$-\frac{3}{2}\sqrt{5}$	3	T_{2u}
14	-4.5	116695	$-\frac{3}{2}\sqrt{5}$	600	all	30	67.5	1	0	1	A_g
15	0	183232	-4.68903	40	all						

TABLE IV: Hamiltonian (1) with $h = 0$ for C_{20} for arbitrary s . The columns list the sector S^z , the first-order degenerate perturbation theory energy correction per spin magnitude $\frac{\Delta E_1}{s}$ on ω (away from the Ising limit $\omega = 0$), its degeneracy (deg.), and the irreducible representation (irrep.) of the I_h symmetry group it belongs. ΔE_1 has been calculated with double-precision accuracy but less digits are shown.

S^z	$\frac{\Delta E_1}{s}$	deg.	irrep.
$Ns - 6$	-7.37374	1	A_g
$Ns - 5$	-7.08838	4	F_g
$Ns - 4$	-7.18588	1	A_u
$Ns - 3$	-6.05876	3	T_{1u}
$Ns - 2$	-4.26553	5	H_g
$Ns - 1$	$-\sqrt{5}$	3	T_{2u}
Ns	0	1	A_g

TABLE V: Maximum value ω_{max} for different s for which the ground state of Hamiltonian (1) for C_{20} has a $\Delta S^z = 2$ magnetization discontinuity between $S^z = Ns - 6$ and $Ns - 4$. The jump does not survive at the isotropic Heisenberg limit $\omega = \frac{\pi}{4}$ for $s > 1$.

s	$\omega_{max}(\pi)$
$\frac{1}{2}$	0.68562
1	0.26685
$\frac{3}{2}$	0.12745
2	0.08186
$\frac{5}{2}$	0.06007
3	0.04739

TABLE VI: Hamiltonian (1) with $h = 0$ for C_{60} for arbitrary s and three different values of $\phi = \tan^{-1} \frac{J_2}{J_1}$ that determines the relative strength of the symmetrically independent exchange interactions. $\phi = \frac{\pi}{50}$ is close to the isolated pentagon limit $J_2 \ll J_1$, $\phi = \frac{\pi}{4}$ corresponds to uniform exchange interactions, and $\phi = \frac{49}{100}\pi$ is close to the dimer limit $J_2 \gg J_1$. The columns list the sector S^z (with saturation value Ns), and for each ϕ value the first-order degenerate perturbation theory energy correction per spin magnitude $\frac{\Delta E_1}{s}$ on ω (away from the Ising limit $\omega = 0$), its degeneracy (deg.), and the irreducible representation (irrep.) of the I_h symmetry group it belongs. ΔE_1 has been calculated with double-precision accuracy but less digits are shown.

S^z	$\phi = \frac{\pi}{50}$			$\phi = \frac{\pi}{4}$			$\phi = \frac{49}{100}\pi$		
	$\frac{\Delta E_1}{s}$	deg.	irrep.	$\frac{\Delta E_1}{s}$	deg.	irrep.	$\frac{\Delta E_1}{s}$	deg.	irrep.
$Ns - 7$	-11.41820	4	F_u	-11.43936	4	F_u	-7.19164	4	F_u
$Ns - 6$	-9.89498	1	A_g	-10.22177	1	A_g	-6.20833	1	A_g
$Ns - 5$	-8.28299	4	F_u	-8.69749	3	T_{1g}	-5.19086	4	F_u
$Ns - 4$	-6.67365	1	A_u	-7.19834	1	A_u	-4.17734	1	A_u
$Ns - 3$	-5.01822	3	T_{1g}	-5.46684	3	T_{1g}	-3.14149	3	T_{1g}
$Ns - 2$	-3.35042	5	H_g	-3.67399	5	H_g	-2.09766	5	H_g
$Ns - 1$	-1.67763	3	T_{2g}	-1.85123	3	T_{2g}	-1.05033	3	T_{2g}
Ns	0	1	A_g	0	1	A_g	0	1	A_g

TABLE VII: Maximum value ω_{max} for which the $s = \frac{1}{2}$, 1, and $\frac{3}{2}$ ground state of Hamiltonian (1) for C_{60} has a $\Delta S^z = 2$ magnetization discontinuity between $S^z = Ns - 6$ and $Ns - 4$ for different values of $\phi = \tan^{-1} \frac{J_2}{J_1}$, which determines the relative strength of the two symmetrically independent exchange interactions. The values for $0.5\pi^-$ are found from first-order perturbation theory on the dimer limit $\phi = \frac{\pi}{2}$ (Table XIII).

$\phi(\pi)$	$\omega_{max}(s = \frac{1}{2})(\pi)$	$\omega_{max}(s = 1)(\pi)$	$\omega_{max}(s = \frac{3}{2})(\pi)$
0.001	0.10693	0.05497	0.03684
0.01	0.10558	0.05385	0.03598
0.05	0.10358	0.05114	0.03375
0.1	0.11293	0.05304	0.03439
0.15	0.14775	0.06311	0.03971
0.2	0.23722	0.08522	0.05109
0.25	0.37183	0.11856	0.06764
0.3	0.46865	0.15763	0.08718
0.35	0.51236	0.20175	0.11042
0.4	0.52813	0.25949	0.14385
0.45	0.54835	0.33235	0.20304
0.49	0.57578	0.51511	0.42140
0.495	0.58107	0.56995	0.51947
0.496	0.58223	0.58366	0.54571
0.497	0.58342	0.59883	0.57525
0.498	0.58464	0.61600	0.60929
0.499	0.58591	0.63632	0.65086
0.5 ⁻	0.58723	0.66303	0.72301

TABLE VIII: Minimum value ω_{min} for which the $s = \frac{1}{2}$, 1, and $\frac{3}{2}$ ground state of Hamiltonian (1) for C_{60} has a $\Delta S^z = 2$ magnetization discontinuity between $S^z = Ns - 6$ and $Ns - 4$ for different values of $\phi = \tan^{-1} \frac{J_2}{J_1}$, which determines the relative strength of the two symmetrically independent exchange interactions. For $\phi \geq 0.01143\pi$ it is $\omega_{min} = 0$ for arbitrary s .

$\phi(\pi)$	$\omega_{min}(s = \frac{1}{2})(\pi)$	$\omega_{min}(s = 1)(\pi)$	$\omega_{min}(s = \frac{3}{2})(\pi)$
0.001	0.00681	0.00341	0.00227
0.01	0.00089	0.00044	0.00030

TABLE IX: Minimum value ϕ_{min} as a function of s for which the ground state of Hamiltonian (1) for C_{60} has a $\Delta S^z = 2$ magnetization discontinuity between $S^z = Ns - 6$ and $Ns - 4$ at the isotropic Heisenberg limit $\omega = \frac{\pi}{4}$.

s	$\phi_{min}(\pi)$
$\frac{1}{2}$	0.20503
1	0.39310
$\frac{3}{2}$	0.46766
2	0.48299
$\frac{5}{2}$	0.48894

TABLE X: First-order degenerate perturbation theory correction of the energy ΔE_1 for the different S^z sectors of C_{60} away from the dimer limit $\phi = \frac{\pi}{2}$ at the antiferromagnetic isotropic Heisenberg limit $\omega = \frac{\pi}{4}$ of Hamiltonian (1) for $h = 0$ and $s = \frac{1}{2}$.

S^z	ΔE_1	S^z	ΔE_1	S^z	ΔE_1	S^z	ΔE_1
0	0	8	-3.37593	16	-2.17645	24	3.44460
1	$-\frac{\sqrt{2}}{8}(\sqrt{5} + 1)$	9	-3.51988	17	-1.75230	25	4.55445
2	-1.12036	10	-3.61148	18	-1.25823	26	5.63228
3	-1.64789	11	-3.52543	19	-0.69700	27	6.83739
4	-2.14589	12	-3.37955	20	-0.07595	28	8.07203
5	-2.51661	13	-3.16651	21	0.72276	29	$\frac{\sqrt{2}}{8}(55 - \sqrt{5})$
6	-2.91936	14	-2.88356	22	1.57382	30	$\frac{15}{2}\sqrt{2}$
7	-3.17653	15	-2.54002	23	2.48032		

TABLE XI: Same as Tab. X for $s = 1$.

S^z	ΔE_1	S^z	ΔE_1	S^z	ΔE_1	S^z	ΔE_1
0	0	16	-9.90661	31	10.16959	46	15.11256
1	$-\frac{\sqrt{2}}{3}(\sqrt{5} + 1)$	17	-9.41163	32	9.77693	47	16.28654
2	-2.99310	18	-8.77918	33	9.42314	48	17.57092
3	-4.40984	19	-8.01996	34	9.11786	49	18.95782
4	-5.76557	20	-7.14364	35	9.03347	50	20.43860
5	-6.83962	21	-5.92341	36	8.90460	51	22.19653
6	-7.96525	22	-4.58861	37	9.00707	52	24.04421
7	-8.80401	23	-3.14716	38	9.19497	53	25.97763
8	-9.53836	24	-1.60129	39	9.46861	54	27.99649
9	-10.16605	25	0.23145	40	9.83200	55	30.24667
10	-10.67917	26	2.01260	41	10.47254	56	32.45238
11	-10.84838	27	4.07544	42	11.20696	57	34.87899
12	-10.90051	28	6.19929	43	12.04390	58	37.35409
13	-10.82584	29	$\frac{\sqrt{2}}{3}(20 - \sqrt{5})$	44	12.99124	59	39.86807
14	-10.61371	30	$\frac{15}{2}\sqrt{2}$	45	14.03629	60	$30\sqrt{2}$
15	-10.27938						

TABLE XII: Same as Tab. X for $s = \frac{3}{2}$.

S^z	ΔE_1	S^z	ΔE_1	S^z	ΔE_1	S^z	ΔE_1
0	0	23	-11.04769	46	2.08329	69	43.65523
1	$-\frac{5\sqrt{2}}{8}(\sqrt{5} + 1)$	24	-8.67899	47	3.37494	70	44.47147
2	-5.61564	25	-5.83354	48	4.89081	71	45.66505
3	-8.27830	26	-3.05808	49	6.61187	72	46.98738
4	-10.83625	27	0.20699	50	8.52480	73	48.44870
5	-12.90461	28	3.57675	51	10.99590	74	50.06102
6	-15.04295	29	$\frac{\sqrt{2}}{8}(51 - 5\sqrt{5})$	52	13.66065	75	51.80777
7	-16.70454	30	$\frac{15}{2}\sqrt{2}$	53	16.49980	76	53.59655
8	-18.19429	31	8.56781	54	19.50498	77	55.51977
9	-19.50325	32	6.62997	55	22.97068	78	57.59398
10	-20.61117	33	4.78123	56	26.36796	79	59.80719
11	-21.14082	34	3.03344	57	30.23707	80	62.14914
12	-21.47156	35	1.75747	58	34.20713	81	64.86843
13	-21.58974	36	0.41310	59	38.26630	82	67.71467
14	-21.47556	37	-0.47076	60	$30\sqrt{2}$	83	70.67810
15	-21.15379	38	-1.18859	61	42.12444	84	73.75551
16	-20.76846	39	-1.73202	62	41.88711	85	77.14699
17	-20.17553	40	-2.08180	63	41.70662	86	80.48426
18	-19.35024	41	-1.87341	64	41.59339	87	84.13303
19	-18.31239	42	-1.47315	65	41.79165	88	87.84905
20	-17.07563	43	-0.86770	66	41.93570	89	91.62191
21	-15.26061	44	-0.03803	67	42.39383	90	$\frac{135}{2}\sqrt{2}$
22	-13.24454	45	0.99192	68	42.96594		

TABLE XIII: Maximum value ω_{max} for which the $s = \frac{1}{2}$, 1, and $\frac{3}{2}$ first-order degenerate perturbation theory ground state of Hamiltonian (1) for C_{60} away from the dimer limit $\phi = \frac{\pi}{2}$ has $\Delta S^z = 2$ magnetization discontinuities, where the sectors $S^z = \frac{N}{2}i + 5$ and $\frac{N}{2}(i + 1) - 5$ with $i = 0, 1, \dots, 2s - 1$ never include the ground state in the external field h .

s	i	$\omega_{max}(\pi)$
$\frac{1}{2}$	0	0.58723
1	0	0.72291
1	1	0.66303
$\frac{3}{2}$	0	0.75-
$\frac{3}{2}$	1	0.75-
$\frac{3}{2}$	2	0.72301

V. CONCLUSIONS

In this paper it was shown that the $\Delta S^z = 2$ quantum magnetization discontinuity of the isotropic quantum antiferromagnetic Heisenberg model on C_{20} in an external field can be continuously traced to a strong discontinuity present at the Ising limit of the model for finite s . This discontinuity originates from the special connectivity of the dodecahedron. C_{60} , which also has I_h symmetry, inherits the discontinuity also at the isotropic limit for sufficiently strong interpentagon interactions. Perturbing away from the limit of infinitely strong interpentagon interactions the number of $\Delta S^z = 2$ discontinuities equals $4s$, and these discontinuities are expected to survive at least close to this limit.

Since the $N = 80$ I_h -symmetry fullerene, the chamfered dodecahedron [1], also has a jump in a magnetic field for $s = \frac{1}{2}$ when its two symmetrically unique interactions are equal [30], it is expected that bigger molecules with the same symmetry will follow the $\Delta S^z = 2$ discontinuity pattern of C_{60} . In their case the interpentagon coupling depends on the strength of exchange interactions of one or more kinds.

The results of the paper show how the magnetization response is determined by the spatial symmetry for the I_h fullerene molecules. The twelve pentagons are distributed according to a specific symmetry that is directly connected with how the spins react to an external magnetic field. This can lead to the prediction of the magnetic properties of large molecules, which are computationally intractable, through the treatment of their smaller symmetric relatives. Especially at

the strong-coupling limit of the twelve pentagons perturbation theory can generate the magnetic response for the whole S^z range, and not only for the higher S^z numbers, which are accessible with Lanczos diagonalization. The response at the dimer limit provides insights into the magnetization response at least close to this limit, as has been shown for the $\Delta S^z = 2$ discontinuity close to saturation. It is highly desirable to find correlations between magnetic behavior and spatial symmetry [11, 27, 29, 30, 51, 52]. In addition, and since the AHM is the large- U limit of the Hubbard model at half-filling [17, 18], it is expected that the I_h -symmetry fullerene molecules will share properties related to strongly-correlated models of itinerant electrons, at least for some range of their parameters.

Appendix A: Degenerate Perturbation Theory on the Intrapentagon Coupling for C_{60}

As an example, the case $s = 1$ is considered. The interaction between nearest-neighbor spins belonging to different pentagons is given by the term inside the brackets in Hamiltonian (1) and $0 \leq \omega < \frac{3}{4}\pi$ is taken. The lowest energies of these dimers in the different S_{dimer}^z sectors are

$$\begin{aligned} S_{dimer}^z = 0, & \quad e_0 = -\frac{1}{2} \left(\cos \omega + \sqrt{1 + 7 \sin^2 \omega} \right), \\ S_{dimer}^z = 1, & \quad e_1 = -\sin \omega, \\ S_{dimer}^z = 2, & \quad e_2 = \cos \omega. \end{aligned} \tag{A.1}$$

It is $e_0 < e_1 < e_2$ for $0 \leq \omega < \frac{3}{4}\pi$. The corresponding dimer eigenstates are called $|0 \rangle$, $|1 \rangle$, and $|2 \rangle$ respectively. The unperturbed Hamiltonian (1) at the $\phi = \frac{\pi}{2}$ -limit for C_{60} has only the interpentagon bonds different from zero, resulting in isolated dimers. The lowest-energy unperturbed states for the different S^z sectors are given as sets of the number of dimers found in each one of the three different dimer eigenstates ($\#$ in $|0 \rangle, \#$ in $|1 \rangle, \#$ in $|2 \rangle$) = (n_0, n_1, n_2) (Table XIV). The corresponding unperturbed energies are $E_0(S^z) = n_0 e_0 + n_1 e_1 + n_2 e_2$. Interdimer interactions, which are nearest-neighbor intrapentagon interactions, are taken as a perturbation to the $\phi = \frac{\pi}{2}$ -limit of Hamiltonian (1). Tables X, XI, and XII list the first-order degenerate perturbation theory energy corrections ΔE_1 of the intrapentagon bonds on the $\phi = \frac{\pi}{2}$ -dimer limit of Hamiltonian (1) for $s = \frac{1}{2}, 1$, and $\frac{3}{2}$ at the isotropic Heisenberg limit $\omega = \frac{\pi}{4}$.

Within first-order perturbation theory the lowest-energy levels in the different S^z sectors are given as $E_0(S^z) + \Delta E_1(S^z)\lambda$, with $\lambda \equiv \frac{J_1}{J_2}$ the perturbation parameter away from the dimer limit. The difference between successive unperturbed energies $E_0(S^z + 1) - E_0(S^z)$ is the same for $\frac{N}{2}i \leq S^z \leq \frac{N}{2}(i + 1) - 1$, $i = 0, 1, \dots, 2s - 1$. For $s = 1$ there are two such S^z ranges, one between

$S^z = 0$ to 30 and the second between $S^z = 30$ and 60 (Fig. 11(b)). At the borders between these $2s$ regions the magnetization step $\Delta S^z = 1$, due to the unperturbed energies. Within first-order perturbation theory the magnitude of ΔS^z within the $2s$ regions is determined by the difference in the perturbative energy corrections between successive sectors $[\Delta E_1(S^z + 1) - \Delta E_1(S^z)]\lambda = \delta(\Delta E_1)\lambda$, which is taken to correspond to the middle point $S^z + \frac{1}{2}$. These differences are symmetric with respect to the center of each region, with symmetrically placed differences adding up to $\frac{2i+1}{\sqrt{2}}$. This is a manifestation of the hole-particle symmetry with respect to the center of the region, after the projection to the lowest-energy dimer states has been made. If these differences do not increase with S^z the magnetization step $\Delta S^z > 1$. According to Tables X, XI, and XII and Fig. 11 there are $4s$ discontinuities for a specific s , with the sectors $S^z = \frac{N}{2}i + 5$ and $S^z = \frac{N}{2}(i + 1) - 5$ with $i = 0, 1, \dots, 2s - 1$ never including the ground state in a magnetic field. These are sectors whose S^z value differs by 5 from the sectors $S^z = \frac{N}{2}i$, with $i = 0, 1, \dots, 2s$. Table XIII lists the ω_{max} values for the $4s$ discontinuities for every s , with each value belonging to a pair of discontinuities.

TABLE XIV: Lowest-energy unperturbed states for Hamiltonian (1) for the truncated icosahedron for $\phi = \frac{\pi}{2}$ and $s = 1$ as a function of S^z given as sets of the number of dimers found in each one of the three different dimer eigenstates ($\#$ in $|0\rangle, \#$ in $|1\rangle, \#$ in $|2\rangle$) = (n_0, n_1, n_2) , and their number.

S^z	dimer eigenstate types	number of states
60	(0,0,30)	1
59	(0,1,29)	30
58	(0,2,28)	435
57	(0,3,27)	4060
56	(0,4,26)	27405
55	(0,5,25)	142506
54	(0,6,24)	593775
\vdots	\vdots	\vdots
32	(0,28,2)	435
31	(0,29,1)	30
30	(0,30,0)	1
29	(1,29,0)	30
28	(2,28,0)	435
27	(3,27,0)	4060
26	(4,26,0)	27405
25	(5,25,0)	142506
24	(6,24,0)	593775
\vdots	\vdots	\vdots
2	(28,2,0)	435
1	(29,1,0)	30
0	(30,0,0)	1

-
- [1] P. W. Fowler and D. E. Manolopoulos, *An atlas of fullerenes*, Oxford University Press, UK, ISBN 9780486453620 (1995), doi:10.1080/10641229608001575.
- [2] H. W. Kroto, *The stability of the fullerenes C_n , with $n = 24, 28, 32, 36, 50, 60$ and 70* , Nature **329**, 529 (1987), doi:10.1038/329529a0.
- [3] H. W. Kroto, J. R. Heath, S. C. O'Brien, R. F. Curl and R. E. Smalley, *C_{60} : Buckminsterfullerene*, Nature **318**, 162 (1985), doi:10.1038/318162a0.

- [4] B. W. Smith, M. Monthieux and D. E. Luzzi, *Encapsulated C_{60} in carbon nanotubes*, Nature **396**, 323 (1998), doi:10.1038/24521.
- [5] H. L. Zhang, W. Chen, L. Chen, H. Huang, X. S. Wang, J. Yuhara and A. Thye Shen Wee, *C_{60} molecular chains on α -sexithiophene nanostripes*, Small **3**, 2015 (2007), doi:10.1002/sml.200700381.
- [6] A. Tamai, W. Auwärter, C. Cepek, F. Baumberger, T. Greber and J. Osterwalder, *One-dimensional chains of C_{60} molecules on $Cu(2 \times 2 \times 1)$* , Surf. Sci. **566-568**, 633 (2004), doi:10.1016/j.susc.2004.06.127.
- [7] C. Zeng, B. Wang, B. Li, H. Wang and J. G. Hou, *Self-assembly of one-dimensional molecular and atomic chains using striped alkanethiol structures as templates*, Appl. Phys. Lett. **79**, 1685 (2001), doi:10.1063/1.1402648.
- [8] C. Chen, H. Zheng, A. Mills, J. R. Heflin and C. Tao, *Temperature evolution of quasi-one-dimensional C_{60} nanostructures on rippled graphene*, Sci. Rep. **5**, 14336 (2015), doi:10.1038/srep14336.
- [9] N. A. Modine and E. Kaxiras, *Variational Hilbert-space-truncation approach to quantum Heisenberg antiferromagnets on frustrated clusters*, Phys. Rev. B **53**, 2546 (1996), doi:10.1103/PhysRevB.53.2546.
- [10] A. F. Hebard et al., *Superconductivity at 18 K in potassium-doped C_{60}* , Nature **350**, 600 (1991), doi:10.1038/350600a0.
- [11] N. P. Konstantinidis, *Capped carbon nanotubes with a number of ground state magnetization discontinuities increasing with their size*, J. Phys. Condens. Matter **29**, 215803 (2017), doi:10.1088/1361-648X/aa6bd4.
- [12] S. Chakravarty, M. P. Gelfand and S. Kivelson, *Electronic correlation effects and superconductivity in doped fullerenes*, Science **254**, 970 (1991), doi:10.1126/science.254.5034.970.
- [13] G. Stollhoff, *Anomalous electron-lattice coupling in C_{60}* , Phys. Rev. B **44**, 10998 (1991), doi:10.1103/PhysRevB.44.10998.
- [14] F. Lin, E. S. Sørensen, C. Kallin and A. J. Berlinsky, *Single-particle excitation spectra of C_{60} molecules and monolayers*, Phys. Rev. B **75**, 075112 (2007), doi:10.1103/PhysRevB.75.075112.
- [15] C. A. Jiménez-Hoyos, R. Rodríguez-Guzmán and G. E. Scuseria, *Polyradical character and spin frustration in fullerene molecules: An ab initio non-collinear Hartree-Fock study*, J. Phys. Chem. A **118**, 9925 (2014), doi:10.1021/jp508383z.
- [16] D. Coffey and S. A. Trugman, *Magnetic properties of undoped C_{60}* , Phys. Rev. Lett. **69**, 176 (1992), doi:10.1103/PhysRevLett.69.176.
- [17] A. Auerbach, *Interacting electrons and quantum magnetism*, Springer New York, USA, ISBN 9781461269281 (1994), doi:10.1007/978-1-4612-0869-3.
- [18] P. Fazekas, *Lecture notes on electron correlation and magnetism*, World Scientific, Singapore, ISBN 9789810224745 (1999), doi:10.1142/2945.
- [19] C. Lhuillier and G. Misguich, *Frustrated quantum magnets*, in *High magnetic field*, Springer Berlin Heidelberg, Berlin, Heidelberg, ISBN 9783540439790 (2002), doi:10.1007/3-540-45649-X.6.
- [20] H. T. Diep, *Frustrated spin systems*, World Scientific, Singapore, ISBN 9789814440738 (2012), doi:10.1142/8676.

- [21] A. P. Ramirez, *Geometrically frustrated matter—magnets to molecules*, MRS Bull. **30**, 447 (2005), doi:10.1557/mrs2005.122.
- [22] J. Schnack, *Effects of frustration on magnetic molecules: A survey from Olivier Kahn until today*, Dalton Trans. **39**, 4677 (2010), doi:10.1039/B925358K.
- [23] Plato, *Timaeus*.
- [24] H. Prinzbach et al., *Gas-phase production and photoelectron spectroscopy of the smallest fullerene, C₂₀*, Nature **407**, 60 (2000), doi:10.1038/35024037.
- [25] Z. Wang et al., *A new carbon solid made of the world's smallest caged fullerene C₂₀*, Phys. Lett. A **280**, 351 (2001), doi:10.1016/S0375-9601(00)00847-1.
- [26] Z. Iqbal et al., *Evidence for a solid phase of dodecahedral C₂₀*, Eur. Phys. J. B **31**, 509 (2003), doi:10.1140/epjb/e2003-00060-4.
- [27] N. P. Konstantinidis, *Competition between frustration and spin dimensionality in the classical antiferromagnetic n-vector model with arbitrary n*, SciPost Phys. Core **6**, 042 (2023), doi:10.21468/SciPostPhysCore.6.2.042.
- [28] R. Rausch, C. Plorin and M. Peschke, *The antiferromagnetic S = 1/2 Heisenberg model on the C₆₀ fullerene geometry*, SciPost Phys. **10**, 087 (2021), doi:10.21468/SciPostPhys.10.4.087.
- [29] N. P. Konstantinidis, *Antiferromagnetic Heisenberg model on clusters with icosahedral symmetry*, Phys. Rev. B **72**, 064453 (2005), doi:10.1103/PhysRevB.72.064453.
- [30] N. P. Konstantinidis, *Unconventional magnetic properties of the icosahedral symmetry antiferromagnetic Heisenberg model*, Phys. Rev. B **76**, 104434 (2007), doi:10.1103/PhysRevB.76.104434.
- [31] N. P. Konstantinidis, *s = 1/2 antiferromagnetic Heisenberg model on fullerene-type symmetry clusters*, Phys. Rev. B **80**, 134427 (2009), doi:10.1103/PhysRevB.80.134427.
- [32] N. P. Konstantinidis, *Zero-temperature magnetic response of small fullerene molecules at the classical and full quantum limit*, J. Magn. Magn. Mater. **449**, 55 (2018), doi:10.1016/j.jmmm.2017.09.020.
- [33] J. Schulenburg, A. Honecker, J. Schnack, J. Richter and H.-J. Schmidt, *Macroscopic magnetization jumps due to independent magnons in frustrated quantum spin lattices*, Phys. Rev. Lett. **88**, 167207 (2002), doi:10.1103/PhysRevLett.88.167207.
- [34] J. Richter, J. Schulenburg, A. Honecker, J. Schnack and H.-J. Schmidt, *Exact eigenstates and macroscopic magnetization jumps in strongly frustrated spin lattices*, J. Phys. Condens. Matter **16**, S779 (2004), doi:10.1088/0953-8984/16/11/029.
- [35] J. Schnack, H.-J. Schmidt, A. Honecker, J. Schulenburg and J. Richter, *Exact eigenstates of highly frustrated spin lattices probed in high fields*, J. Phys. Conf. Ser. **51**, 43 (2006), doi:10.1088/1742-6596/51/1/007.
- [36] H. Nakano and T. Sakai, *The two-dimensional S=1/2 Heisenberg antiferromagnet on the Shuriken lattice -a lattice composed of vertex-sharing triangles-*, J. Phys. Soc. Jpn. **82**, 083709 (2013), doi:10.7566/JPSJ.82.083709.
- [37] H. Nakano, M. Isoda and T. Sakai, *Magnetization process of the S = 1/2 Heisenberg antiferromagnet*

- on the Cairo pentagon lattice, J. Phys. Soc. Jpn. **83**, 053702 (2014), doi:10.7566/JPSJ.83.053702.
- [38] H. Nakano, T. Sakai and Y. Hasegawa, *Spin-flop phenomenon of two-dimensional frustrated antiferromagnets without anisotropy in spin space*, J. Phys. Soc. Jpn. **83**, 084709 (2014), doi:10.7566/JPSJ.83.084709.
- [39] R. Furuchi, H. Nakano, N. Todoroki and T. Sakai, *Magnetization process of the $S = 1/2$ Heisenberg antiferromagnet on the floret pentagonal lattice*, J. Phys. Commun. **5**, 125008 (2021), doi:10.1088/2399-6528/ac3f7a.
- [40] R. Furuchi, H. Nakano and T. Sakai, *Numerical study of $S=1/2$ Heisenberg antiferromagnet on the floret pentagonal lattice*, JPS Conf. Proc. **38**, 011167 (2023), doi:10.7566/JPSCP.38.011167.
- [41] C. Schröder, H.-J. Schmidt, J. Schnack and M. Luban, *Metamagnetic phase transition of the antiferromagnetic Heisenberg icosahedron*, Phys. Rev. Lett. **94**, 207203 (2005), doi:10.1103/PhysRevLett.94.207203.
- [42] N. P. Konstantinidis, *Antiferromagnetic Heisenberg model on the icosahedron: Influence of connectivity and the transition from the classical to the quantum limit*, J. Phys. Condens. Matter **27**, 076001 (2015), doi:10.1088/0953-8984/27/7/076001.
- [43] K. Karřiová, J. Strečka and J. Richter, *Enhanced magnetocaloric effect in the proximity of magnetization steps and jumps of spin-1/2 XXZ Heisenberg regular polyhedra*, J. Phys. Condens. Matter **29**, 125802 (2017), doi:10.1088/1361-648X/aa53ab.
- [44] F. Mila, *Ladders in a magnetic field: A strong coupling approach*, Eur. Phys. J. B **6**, 201 (1998), doi:10.1007/s100510050542.
- [45] M. Jaime et al., *Magnetic-field-induced condensation of triplons in the purple pigment $BaCuSi_2O_6$* , Phys. Rev. Lett. **93**, 087203 (2004), doi:10.1103/PhysRevLett.93.087203.
- [46] X.-G. Zhou et al., *Particle-hole symmetry breaking in a spin-dimer system $TlCuCl_3$ observed at 100 T*, Phys. Rev. Lett. **125**, 267207 (2020), doi:10.1103/PhysRevLett.125.267207.
- [47] M. P. Gelfand, *Series expansions for excited states of quantum lattice models*, Solid State Commun. **98**, 11 (1996), doi:10.1016/0038-1098(96)00051-8.
- [48] N. P. Konstantinidis and D. Coffey, *Accurate results from perturbation theory for strongly frustrated $S = \frac{1}{2}$ Heisenberg spin clusters*, Phys. Rev. B **63**, 184436 (2001), doi:10.1103/PhysRevB.63.184436.
- [49] S. L. Altmann and P. Herzig, *Point-group theory tables*, Oxford University Press, UK, ISBN 9780198552260 (1994).
- [50] P. R. Cromwell, *Polyhedra*, Cambridge University Press, UK, ISBN 9780521664059 (1997).
- [51] A. Machens, N. P. Konstantinidis, O. Waldmann, I. Schneider and S. Eggert, *Even-odd effect in short antiferromagnetic Heisenberg chains*, Phys. Rev. B **87**, 144409 (2013), doi:10.1103/PhysRevB.87.144409.
- [52] N. P. Konstantinidis, *Discontinuous classical ground state magnetic response as an even-odd effect in higher order rotationally invariant exchange interactions*, J. Phys. Commun. **1**, 055027 (2017), doi:10.1088/2399-6528/aa95db.